

Adjoint-based shape and kinematics optimization of flapping wing propulsive efficiency

Martin Jones¹ and Nail K. Yamaleev²

North Carolina A&T State University, Greensboro, NC 27411

Optimization of the 3-D unsteady viscous flow near a flapping wing is performed using a time-dependent adjoint-based methodology developed in [AIAA 2008-5857 and AIAA J. Vol.48, No.6, pp.1195-1206, 2010]. Sensitivities of the thrust and propulsive efficiency to wing shape and kinematic parameters are computed using the time-dependent discrete adjoint formulation. The unsteady discrete adjoint equations required for calculation of the sensitivity derivatives are integrated backward in time over the entire interval of interest. The gradient of the objective functional obtained using the adjoint formulation is then used to update the values of shape and kinematic design variables. The efficiency of this adjoint-based methodology is demonstrated by optimizing shape and kinematics of a wing undergoing insect-based flapping motion. Our numerical results show that the highest improvement in the thrust and propulsive efficiency is obtained by using the combined optimization of wing shape and kinematics.

I. Introduction

Insects and small birds represent fully functional examples of efficient small-scale flying devices. However, copying of wing kinematics and shape of flying animals is far from being sufficient to design and build effective, highly maneuverable, agile micro air vehicles (MAVs). Indeed, the current state-of-the-art materials, micro-scale actuators, propulsion systems, and power sources are different and in most cases less efficient than those created by Mother Nature over millions years of evolution. This lack in efficiency of currently available MAV components indicates that a different region of the design space than that associated with flying insects and animals should be explored to be able to maximize the performance of flapping-wing microsystems. Therefore, designs inspired by flying animals can be used only as a preliminary conceptual design that requires further optimization for constructing efficient and agile flying micro-scale platforms optimized for size, weight, speed, and maneuverability. This is a very challenging optimization problem that involves hundreds or even thousands kinematics and shape design variables and is governed by highly unsteady vortex-dominated turbulent flows. Therefore, efficient, mathematically rigorous optimization techniques based on optimal control theory should be used for solving this class of problems.

In spite of significant progress in modeling and computational fluid dynamics (CFD) analysis of flapping- and rotary-wing platforms [1-5], questions related to optimal design of efficient micro air vehicles (MAV) have not yet been properly addressed especially in three dimensions because of the complicated physical phenomena and computational cost involved. Various parametric and sensitivity studies (e.g., see [1]) have revealed that there is an essentially nonlinear relationship between the major wing kinematic parameters (amplitude, frequency, phase shift angle), shape parameters (wing planform, twist, and thickness), and global flow parameters (the Reynolds, Strouhal, and Mach numbers). Conventional parametric studies, which estimate the sensitivity to each individual design variable independently, do not take into account this nonlinear relationship between the main parameters determining the MAV performance. Furthermore, parametric studies are extremely computationally expensive because of the very large dimensionality of the design space and therefore impractical for optimization and design of efficient flapping-wing microsystems.

Several attempts have recently been made to use genetic algorithms based on low-fidelity models [6], high-fidelity models [7], and experimental apparatus [8] for optimization of flapping-wing flows. Since these stochastic optimization techniques require thousands of evaluations of the objective functional and consequently thousands of solves of the unsteady flow equations for each design variable, all these approaches have been limited to optimization of 2-D flows with a very small number (less than 4) of design variables.

Gradient-based methods provide a powerful alternative for optimization of flapping airfoils and wings. Culbreth et al. [9] uses a finite difference method coupled with a 3-D Navier-Stokes solver to evaluate the

¹ Graduate student, 1601 E. Market St., Greensboro, NC

² Associate Professor, Department of Mathematics, 1601 E. Market St., Greensboro, NC. Senior member AIAA

sensitivities of a modified propulsive efficiency to 4 spanwise twist design variables. In [10], a forward mode differentiation method governed by a 2-D Navier-Stokes solver has been successfully used to maximize thrust and propulsive efficiency of a pitching and plunging airfoil.

Unlike the forward mode differentiation methods used in [9, 10], which suffer from excessive cost caused by the need to solve the unsteady Navier-Stokes equations as many times as the number of design variables, an adjoint method provides the sensitivities at a cost which is comparable to that of a single flow solution and independent of the number of design variables. Adjoint-based optimization of flapping wing flows has been very rare and received significantly less attention [11, 12]. In the present paper the adjoint based methodology developed in [13, 14] is used to optimize the performance of an isolated wing in hover. To our knowledge, this work is the first application of an adjoint-based methodology for *combined optimization of shape and kinematics* of a wing undergoing flapping motion governed by the 3-D unsteady Reynolds-Averaged Navier-Stokes equations. Wing kinematic parameters including stroke, pitch, and heave angle amplitudes, frequencies, and phase shift angles as well as shape parameters describing the planform, twist, and thickness of the wing geometry are used as design variable. Our numerical results show that the wing performance significantly increases while all the imposed constraints are satisfied in the course of optimization, thus indicating that the adjoint-based methodology can be efficiently used for optimization and design of MAV systems.

The rest of the paper is organized as follows. Section II introduces the unsteady governing equations and the numerical method. Moving grids and wing kinematics used in the present analysis are presented in Sections III and IV, respectively. In Section V, we briefly outline a time-dependent adjoint based optimization methodology. Successful demonstrations of this adjoint-based methodology for optimization of shape and kinematics of a flapping wing are presented in Section VI. We summarize and draw conclusions in Section VII.

II. Governing Equations and Numerical Method

The fully turbulent incompressible flow near a wing undergoing an insect-based flapping motion is simulated using the 3-D unsteady Reynolds-Averaged Navier-Stokes (URANS) equations written in the integral conservation law form as follows:

$$\frac{\partial(V\mathbf{Q})}{\partial t} + \oint_{\Gamma} (\mathbf{F}_i - \mathbf{F}_v) \cdot \mathbf{n} dS = \mathbf{0}, \quad (1)$$

where V is a moving control volume bounded by the surface Γ , \mathbf{Q} represents a vector of the volume-averaged primitive variables $\mathbf{Q}=[p, u, v, w]^T$, \mathbf{n} is the outward unit face normal vector, and \mathbf{F}_i and \mathbf{F}_v are the inviscid and viscous flux vectors, respectively. Note that the incompressible continuity equation in Eq. (1) does not have a time derivative. For a moving control volume, the inviscid flux vector must account for the difference in the fluxes due to the movement of control volume faces. Given a flux vector \mathbf{F} on a static grid, the corresponding flux vector \mathbf{F}_i on a moving grid is defined as $\mathbf{F}_i^1 = \mathbf{F}^1 - \mathbf{W} \cdot \mathbf{n}$ and $\mathbf{F}_i^k = \mathbf{F}^k - \mathbf{Q}(\mathbf{W} \cdot \mathbf{n})$ for $k=2, 3, 4$, where \mathbf{W} is a local face velocity. The governing equations are closed with the perfect gas equation of state and the Spalart-Allmaras turbulence model for the eddy viscosity. Note that for the special case of $\mathbf{Q}=\text{const}$, the conservation equations (1) reduce to the Geometric Conservation Law (GCL):

$$\frac{\partial V}{\partial t} + \oint_{\Gamma} \mathbf{W} \cdot \mathbf{n} dS = \mathbf{0}. \quad (2)$$

The GCL provides a precise relation between the rate of change of the time-dependent control volume and its local face velocity \mathbf{W} . Though the GCL equation is a direct consequence of the governing equations (1) and is satisfied at the differential level, this is usually not the case at the discrete level. To preserve a constant solution on dynamic grids, the discrete GCL residual R_{GCL} is added to the discretized flow equations (see [15] for further details).

In the present study, the artificial compressibility form of the governing equations (1) is discretized using a 2nd-order node-centered finite volume scheme [16, 17]. The time derivative is approximated by a 2nd-order backward difference (BDF2) formula. The inviscid fluxes at cell interfaces are computed using Roe's approximate Riemann solver, and the viscous fluxes are approximated by a method equivalent to a 2nd-order finite element Galerkin procedure. The mesh velocity terms are evaluated with the BDF2 formula consistent with the discretization of the time derivative. An approximate solution of the linear system of equations formed within each time step is obtained with a multicolor Gauss-Seidel point-iterative scheme. The turbulence model is integrated all the way to the wall without the use of wall functions and is solved separately from the mean flow equations. The above numerical method implemented in a fully unstructured Reynolds-averaged Navier-Stokes solver, FUN3D, [18] has been used in all numerical studies presented in this paper. The FUN3D solver demonstrates high parallel scalability which is achieved through domain decomposition and message passing communication.

III. Rigidly Moving Grid

To accurately resolve the flow near a wing during the entire flapping motion, a body-fitted mesh is used, so that it moves rigidly along with the wing. The rigid mesh motion is generated by a 4x4 transformation matrix, T , [15]. The transformation matrix enables general translations and rotations of the grid according to the following relation:

$$\mathbf{x} = T\mathbf{x}_0,$$

which moves a point from an initial position (x_0, y_0, z_0) to its new position (x, y, z) :

$$\begin{bmatrix} x \\ y \\ z \\ 1 \end{bmatrix} = \begin{bmatrix} r_{11} & r_{12} & r_{13} & t_x \\ r_{21} & r_{22} & r_{23} & t_y \\ r_{31} & r_{32} & r_{33} & t_z \\ 0 & 0 & 0 & 1 \end{bmatrix} \begin{bmatrix} x_0 \\ y_0 \\ z_0 \\ 1 \end{bmatrix}. \quad (3)$$

In Eq. (3), the 3x3 matrix R defines a general rotation, and the vector $\mathbf{t} = [t_x, t_y, t_z]^T$ specifies a translation. Note that the matrix T depends on time and design variables, \mathbf{D} . One key feature of this approach is that multiple transformations telescope via matrix multiplication. This formulation is particularly attractive for composite parent-child body motion. Herein, rotations associated with the wing pitch and heave motions are specified relative to the stroke motion. For a rigid motion, the grid equation at time level n is defined as follows:

$$\mathbf{G}(\mathbf{X}^0, \mathbf{X}^n, \mathbf{D}) = \mathcal{R}\mathbf{X}^0 + \boldsymbol{\tau} - \mathbf{X}^n, \quad (4)$$

where \mathbf{X}^0 and \mathbf{X}^n are the grid vectors at the initial and n -th time levels, \mathcal{R} is a block-diagonal matrix with 3×3 blocks representing rotation.

IV. Wing Kinematics

In contrast to conventional approaches based on the assumption that flapping motion occurs sinusoidally, in the present analysis three angles associated with the stroke position θ , pitch angle α , and heave angle φ representing the deviation from the mean stroke plane are defined as:

$$\begin{cases} \theta = \sum_{k=1}^s \theta_k P_k^\theta(f_\theta, t) \\ \alpha = \sum_{k=1}^s \alpha_k P_k^\alpha(f_\alpha, t) \\ \varphi = \sum_{k=1}^s \varphi_k P_k^\varphi(f_\varphi, t) \end{cases} \quad (5)$$

where $P_k^\theta, P_k^\alpha, P_k^\varphi$ are periodic splines, f_θ, f_α , and f_φ are stroke, pitch, and heave frequencies, respectively. The use of periodic splines instead of sinusoidal functions significantly enriches the design space, while practically not increasing the total number of design variables. These three angles are used to construct the corresponding rotation matrices of the form given by Eq. (3). These matrices are then multiplied together to form the final rotation matrix used to determine the current wing position.

The rotation associated with the stroke motion occurs with respect to the wing root. Initially, the wing flips (pitches) about an axis located approximately at 38% of the chord from the leading edge. For the baseline configuration, the pitching axis remains in the stroke plane throughout the entire motion, and the forward and backward stroke arcs are kinematically symmetric. Note that for this wing motion, the midpoint of the flip occurs precisely at the end of the forward stroke or the end of the backward stroke. The amplitudes and frequencies in Eq. (5) as well as the coefficients of the periodic splines $P_k^\theta, P_k^\alpha, P_k^\varphi$ are used as design variables

and optimized to maximize the thrust and propulsive efficiency of the flapping wing. Along with the lower and upper bounds for each design variable, the following constraints:

$$f_\theta = f_\alpha = f, \quad f_\varphi = 2f$$

are imposed on the frequencies for all test cases considered.

V. Adjoint-based Time-Dependent Optimization Methodology

To increase the wing performance, an aerodynamic quantity of interest (e.g., thrust, lift, drag, or their combination) is considered as a functional which is maximized by using optimal control theory, thus leading to the following discrete PDE-constrained optimization problem:

$$\left\{ \begin{array}{l} \min F_{\text{obj}}(\mathbf{D}), \quad F_{\text{obj}}(\mathbf{D}) = \sum_{n=N_b}^{N_e} f^n \Delta t, \quad f^n = \sum_{k=1}^K \omega_k (C_k^n - (C_k^n)_{\text{target}})^2 \\ \text{subject to: } V^n \frac{3\mathbf{Q}^n - 4\mathbf{Q}^{n-1} + \mathbf{Q}^{n-2}}{2\Delta t} + \mathbf{R}^n + \mathbf{R}_{GCL}^n \mathbf{Q}^{n-1} = 0 \\ \mathbf{G}^n(\mathbf{X}^0, \mathbf{X}^n, \mathbf{D}) = 0 \end{array} \right. \quad (6)$$

where \mathbf{D} is a vector of design variables, \mathbf{Q}^n is a vector of flow variables, C_k^n is a k -th aerodynamic coefficient such as thrust, lift, drag, or their combination and $(C_k^n)_{\text{target}}$ is its target value, ω_k is a user-defined weighting factor, N_b and N_e are time levels corresponding to a time interval over which the objective functional is minimized, \mathbf{R}^n and \mathbf{G}^n are the flow and grid residuals, and \mathbf{R}_{GCL}^n is the geometric conservation law term.

The discrete time-dependent optimization problem (6) is solved by the method of Lagrange multipliers which is used to enforce the flow and grid equations (1, 4) as constraints. The Lagrangian functional is defined as follows:

$$L(\mathbf{D}, \mathbf{Q}, \mathbf{X}, \Lambda_f, \Lambda_g) = \sum_{n=1}^N f^n \Delta t + \sum_{n=1}^N [\Lambda_f^n]^T \left(V^n \frac{3\mathbf{Q}^n - 4\mathbf{Q}^{n-1} + \mathbf{Q}^{n-2}}{2\Delta t} + \mathbf{R}^n + \mathbf{R}_{GCL}^n \mathbf{Q}^{n-1} \right) \Delta t + \sum_{n=1}^N [\Lambda_g^n]^T \mathbf{G}^n \Delta t \quad (7)$$

where Λ_f^n and Λ_g^n are vectors of Lagrange multipliers associated with the flow and grid equations, respectively, \mathbf{D} is a vector of design variables, and $f^n = 0$ for $n < N_b$ and $n > N_e$. Note that terms corresponding to the initial conditions are omitted in Eq. (7).

Differentiating the Lagrangian with respect to \mathbf{D} , collecting the coefficients of $\partial \mathbf{Q}^n / \partial \mathbf{D}$, and setting them equal to zero, the following equations for the flow adjoint variables Λ_f are derived:

$$\frac{3V^n \Lambda_f^n - 4V^{n+1} \Lambda_f^{n+1} + V^{n+2} \Lambda_f^{n+2}}{2\Delta t} + \left[\frac{\partial \mathbf{R}^n}{\partial \mathbf{Q}^n} \right]^T \Lambda_f^n + \mathbf{R}_{GCL}^n \Lambda_f^{n+1} = - \left[\frac{\partial f^n}{\partial \mathbf{Q}^n} \right]^T \quad (8)$$

The grid adjoint equations are obtained in a similar way (see [14] for details). The key advantage of the adjoint formulation is that the adjoint equations (8) are independent of the vector \mathbf{D} , and should be solved once at each optimization iteration, regardless of the number of design variables. Since the first term in Eq. (8) approximates the negative time derivative, the unsteady adjoint equations have to be integrated backward in time. Therefore, the entire flow solution history should be available during the backward-in-time integration of the flow adjoint equations. In the present approach, the flow variables, grid coordinates, and grid velocities are stored to disk at the end of each time step of the flow solution. During the integration of Eq. (8) in reverse time, the stored data are loaded from disk. With the adjoint variables satisfying the flow and grid adjoint equations, the gradient of the Lagrangian with respect to \mathbf{D} is calculated as follows:

$$\frac{dL}{d\mathbf{D}} = \sum_{n=1}^N \left(\frac{\partial f^n}{\partial \mathbf{D}} + [\Lambda_f^n]^T \left(\frac{\partial \mathbf{R}^n}{\partial \mathbf{D}} + \frac{\partial \mathbf{R}_{GCL}^n}{\partial \mathbf{D}} \mathbf{Q}^{n-1} \right) + [\Lambda_g^n]^T \frac{\partial \mathbf{G}^n}{\partial \mathbf{D}} \right) \Delta t \quad (9)$$

As in Eq. (7), terms corresponding to the initial conditions are omitted. A minimum of the objective functional is found by using a gradient-based optimization package PORT [19].

VI. Results and Discussion

The adjoint-based optimization methodology described above is used to improve the performance of an isolated flapping wing in hover. The baseline wing resembles a wing profile of the fruit fly, *Drosophila melanogaster*. The initial wing geometry has the semi-circular leading and trailing edges, a mean aspect ratio of 2.24, and a thickness-to-chord ratio of 0.04. The hovering wing is assumed to be operating in quiescent conditions. The

baseline Reynolds number based on the wing maximum tip speed is set equal to 2,000. Our numerical experiments have shown no appreciable difference between the turbulent and laminar flow solutions and their adjoints at this relatively small Reynolds number. Therefore, in the present work it is assumed that the flow is laminar. The baseline kinematic motion consists of two rotations each occurring at the reduced frequency of 0.236. The first rotation is a stroke motion with amplitude of $\theta_0 = 60^\circ$. The second rotation is a pitch motion with amplitude of $\alpha_0 = 45^\circ$. The stroke and pitch angles are defined by Eq. (5), where the spline coefficients have been selected such that each rotation very closely approximates a sinusoidal motion. For the baseline configuration, the heave angle is assumed to be zero over the entire period of flapping motion.

A hexahedral mesh consisting of 251,766 nodes has been used in all numerical experiments presented in this paper. To accurately resolve the boundary layer and vortex shedding near the wing during the entire flapping motion, the Arbitrary Lagrangian-Eulerian (ALE) formulation is applied, so that the grid moves rigidly along with the wing. As a result, the highest grid resolution is achieved in the boundary layer and in the vicinity of the wing during the entire period of flapping motion, thus significantly reducing the computational cost.

Three optimization cases are considered in the present study. The first case considers optimization of the wing geometry alone, assuming that the wing kinematics remains fixed and equal to that of the baseline configuration. The second case optimizes only the wing kinematics, so that the geometry of the wing does not change in the course of optimization. The third case is based on the combined optimization of both wing shape and its kinematics. The results obtained for all three cases are compared with each other to evaluate the contribution made by the shape and kinematic design variables and the nonlinear relationship between these parameters.

A proper choice of the objective functional is critical not only for increasing the thrust generated by the wing, but also for minimizing the power required for its operation. Note that maximization of the thrust coefficient alone may also increase the drag, thus indicating that significantly higher power would be required for operating the optimized flapping wing. To overcome this problem, the objective functional f^n in Eq. (6) for all three cases considered has been defined as follows:

$$f^n = (C_x^n - C_{\text{target}}^n)^2 + \omega_1 (C_y^n)^2 + \omega_2 (C_z^n)^2, \quad (10)$$

where ω_1 and ω_2 are weight coefficients which are both set to be 5. Note that the thrust target value is set equal to 10, which is significantly higher than its baseline value. The last two terms in Eq. (10) penalize the objective functional in such a way that the functional rapidly increases if both C_y and C_z deviate from zero, thus minimizing the y - and z -components of the aerodynamic force and reducing the power required for the wing motion in the stroke plane. For all test cases, the wing motion consists of two full strokes. The time levels N_b and N_e , over which the objective functional given by Eq. (6) is minimized, have been chosen such that they correspond to the second full stroke of the baseline configuration.

The 3-D discrete primal and adjoint equations are integrated using the BDF2 scheme with a physical time step corresponding to 150 steps per period of the baseline motion. Forty subiterations are used at each time step. Each simulation is run for 300 time steps and is performed on a workstation with the total of 8 processing cores. Approximately 6 gigabytes of disk space are required to store the entire flow solution history. Individual primal and adjoint solutions require approximately 4 and 3.5 hours of wall-clock time, respectively.

a. Optimization of wing geometry

The first problem is a design optimization of the baseline wing undergoing sinusoidal insect-based flapping motion. In the current study, the wing surface parameterization scheme developed in [20] is employed. This approach uses very general shape parameterizations of existing surface grids based on a set of design variables such as planform, twist, thickness, shear, and camber parameters at various locations on the geometry. In the present work, we use a set of 19 active design variables including 12 variables to control the wing planform and 7 variables to control the twist. The root section of the wing is held fixed in all our optimization studies. Upper and lower bounds on each design variable have been chosen to prevent nonphysical surface shapes. Though this parameterization also allows for wing thickness, camber, and shear variations, these design variables are held fixed for all cases considered.

The convergence history of the objective functional given by Eq. (10) is shown in Fig. 1. The objective functional has been reduced from its initial value of 1295 to a final value of 1280 over 18 design cycles. Note that the major reduction occurs during the first 10 design cycles after which further improvements are negligible. Closer inspection of the final values of the design variables reveals moderate changes to all planform parameters and very slight changes to all twist parameters, thus indicating that the twist has negligible effect on the wing performance.

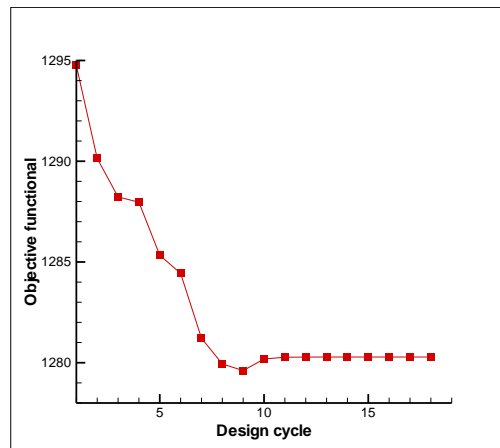


Figure 1: Convergence history of the objective functional for the shape optimization problem.

The baseline and optimized wing geometries are compared in Fig. 8. The optimization has increased the span of the wing by 33%, while reducing the chord length by nearly 25%. Another noticeable difference between the planforms of the wing before and after optimization is a much sharper wing tip of the optimized configuration as compared with that of the baseline geometry. Also, the optimization has slightly increased the twist of the wing across its span.

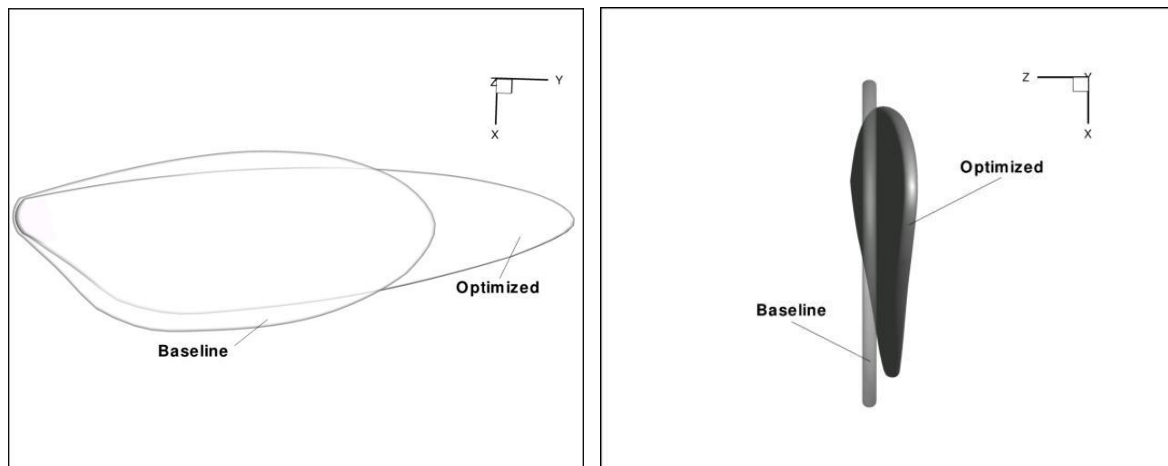


Figure 2: Planforms (left) and cross sections of the wing before and after shape optimization.

The effect of these significant changes in the wing geometry on the flowfield can be seen in Fig. 3 that presents snapshots of an iso-surface of q -criterion obtained for the baseline and optimal wing geometries at four phase angles $\psi = 292.5^\circ, 315^\circ, 337.5^\circ, 360^\circ$ during the second backward stroke. As one can see in Fig. 3, the optimized wing geometry significantly strengthens the leading edge and trailing edge vortices, thus considerably reducing the pressure in the upper surface of the wing and increasing the thrust. Another interesting observation is that the leading edge vortex is present along the entire span of the wing, which explains the increase in the wing span in the course of optimization. As evident in Fig. 3, the sharper is the wing tip, the stronger the vortex it generates over the entire duration of a stroke.

The baseline and optimized thrust profiles are shown in Fig. 4. The mean value of the thrust coefficient has been increased by more than 90% over its baseline value. Note, however, that the increase in the propulsive efficiency is significantly less, as one can see in Fig. 5. In the present study, the propulsive efficiency is evaluated as the thrust-to-drag ratio. As follows from this comparison, the stroke-averaged propulsive efficiency of the optimized configuration is about 10% higher than that obtained for the baseline wing geometry. These results show that shape optimization alone provides only minor improvements in the propulsive efficiency, thus indicating that combined optimization of wing geometry and kinematics is required to significantly increase its performance.

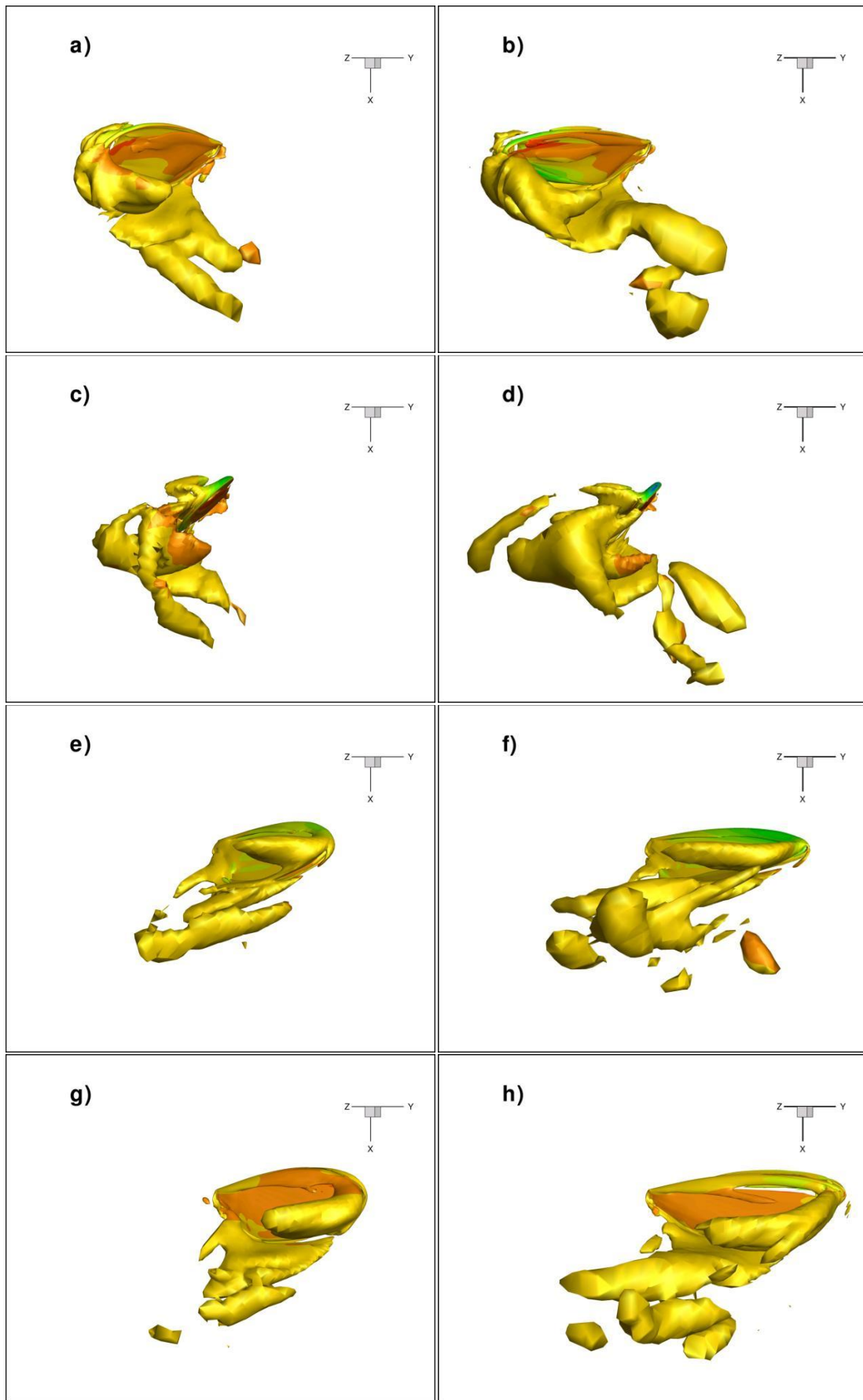


Figure 3: Iso-surface of the q -criterion colored with pressure contours at phase angles $\psi = 292.5^\circ, 315^\circ, 337.5^\circ, 360^\circ$ obtained with the baseline (left column) and optimized wing geometry.

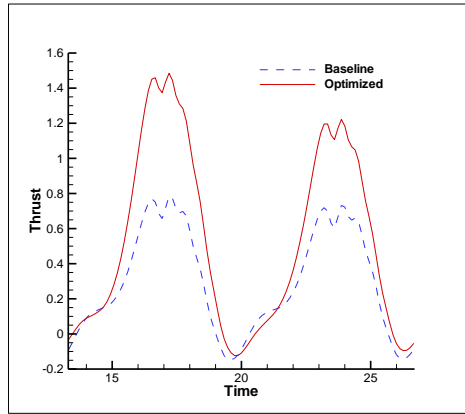


Figure 4: Baseline and optimal thrust profiles.

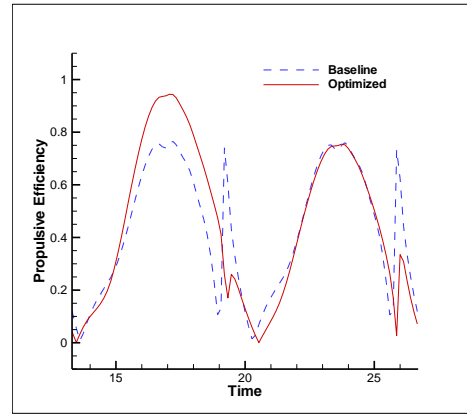


Figure 5: Propulsive efficiency before and after shape optimization.

b. Optimization of wing kinematics

The second problem considers optimization of wing kinematics, which is based on minimization of the same objective functional used in the previous case. The stroke, pitch, and heave angles defining the position of the wing at each moment of time are given by Eq. (5). Coefficients of the periodic splines in Eq. (5), which are associated with the amplitude, frequency, shape, and symmetry of each angle profile, are used as design variables. Thus, there are a total of 8 active kinematic design variables for this test case.

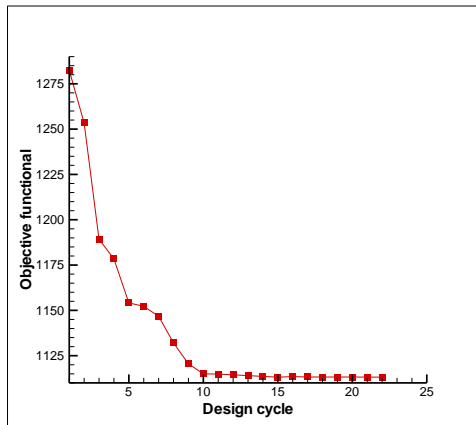


Figure 6: Convergence history of the objective functional.

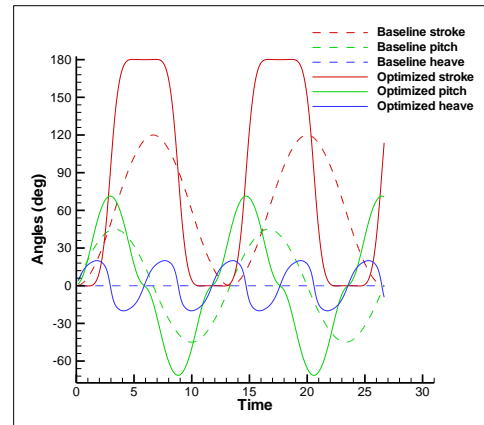


Figure 7: Baseline and optimal stroke, pitch and heave angle profiles.

The convergence history of the objective functional is presented in Fig. 6. The value of the objective functional rapidly drops from 1282 to 1150 over the first 5 design cycles. The objective functional reaches its lowest value of 1113 at the 10th design cycle, after which further improvements are negligible, because many of the design variables have reached their bound constraints. The stroke, pitch, and heave angle profiles before and after the optimization are presented in Fig. 7. The amplitudes of all angles have been significantly increased during the optimization, reaching the values of 90° , 71° , and 20° , respectively. Note that the stroke and heave angles have reached their upper bound values. The optimizer has also increased the stroke, pitch and heave frequencies by 13%, so that they attain their upper bound values. The final values of the other design variables demonstrate moderate changes as compared with their initial values. One of the key distinctions of the optimal kinematics from the baseline kinematics is a significant stroke deviation from the mean stroke plane, which closely resembles a complex figure-eight stroke path observed in biological flyers. Another important observation that can be made from Fig. 7 is that the optimized stroke and pitch angles significantly differ from their baseline sinusoidal profiles. In contrast to the baseline kinematics, the optimal stroke angle profile is nearly flat during stroke reversals and significantly steeper in the middle of each stroke, while the pitch angle demonstrates the opposite behavior.

Snapshots of an iso-surface of q -criterion colored with pressure contours calculated using the baseline and optimized kinematic motions at four phase angles $\psi = 292.5^\circ, 315^\circ, 337.5^\circ, 360^\circ$ are shown in Fig. 8. As in the previous case, the optimization of wing kinematics has led to the significant increase in the size and strength

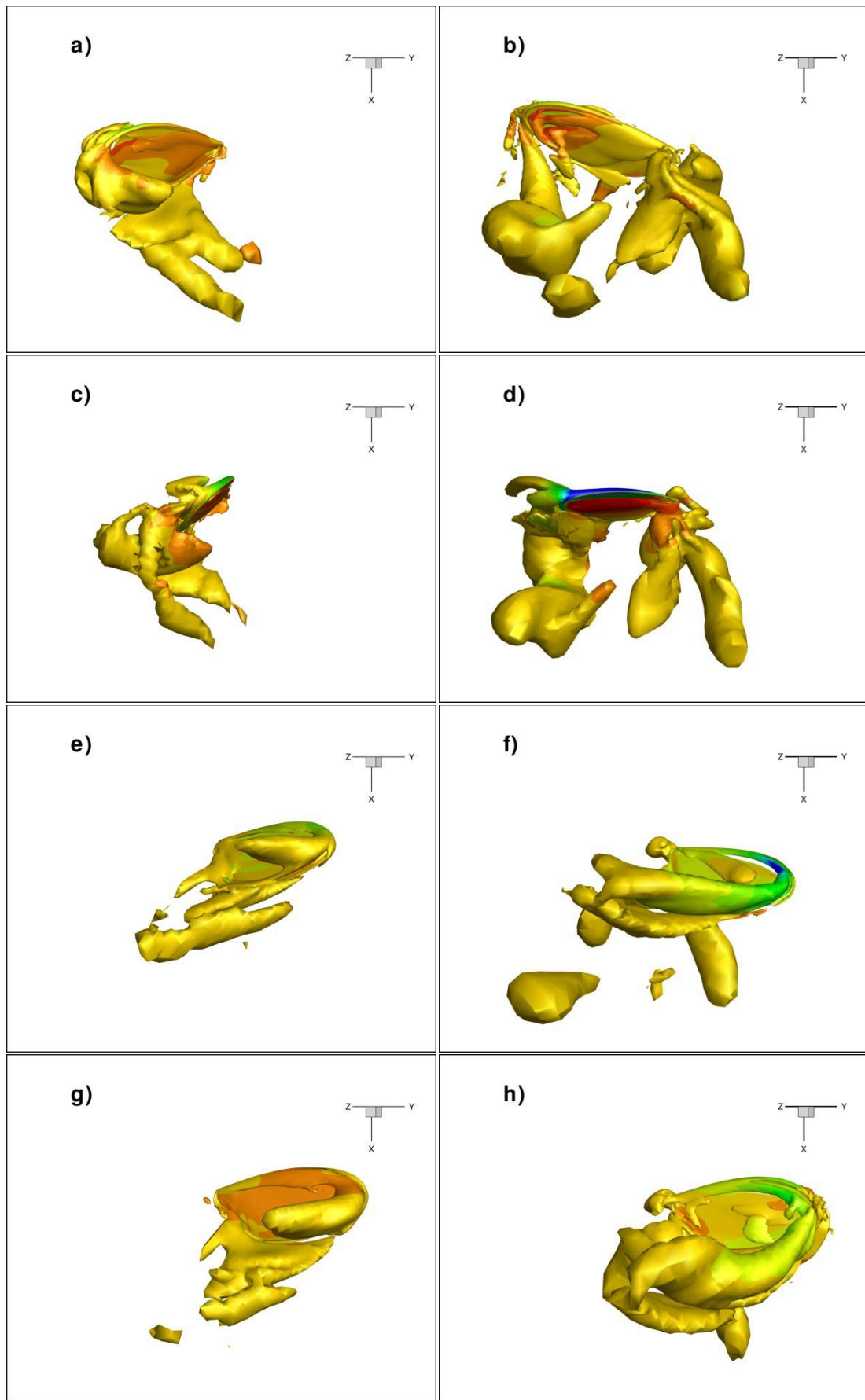


Figure 8: Iso-surface of the q -criterion colored with pressure contours at phase angles $\psi = 292.5^\circ, 315^\circ, 337.5^\circ, 360^\circ$ obtained for the baseline (left column) and optimized wing kinematics.

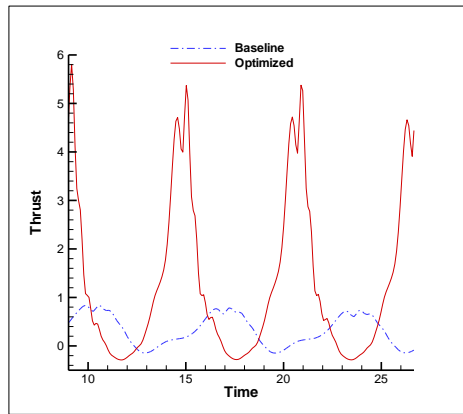


Figure 9: Baseline and optimal thrust profiles.

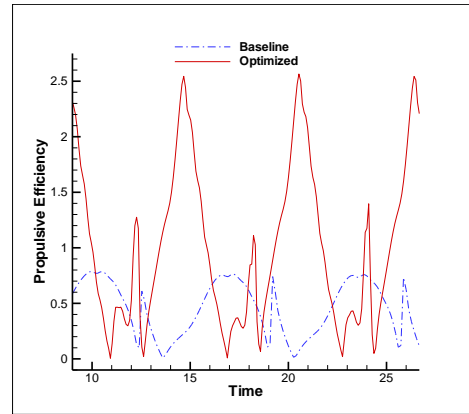


Figure 10: Propulsive efficiency before and after optimization of wing kinematics.

of the leading and trailing edge vortices. One of the reasons for strengthening the leading edge vortex is the increase in the pitch and stroke amplitudes. As one can see in Fig. 8, the 20° deviation from the stroke plane and nearly vertical motion of the wing at the end of each stroke significantly increase the leading edge vortex strength during the transition from upward to backward strokes. The optimized kinematics also strengthens the wake capture effect that generates additional aerodynamic forces during stroke reversals, when the wing rapidly rotates and change direction.

Figure 9 shows the thrust coefficient obtained using the baseline and optimized wing kinematics. As follows from this comparison, the mean value of the thrust coefficient over the second stroke cycle has increased by a factor of 4.5 after the optimization of wing kinematics. In contrast to the shape optimization, the propulsive efficiency provided by the optimized wing kinematics is significantly higher than that of the baseline configuration, as evident in Fig. 10. The mean-stroke value of the propulsive efficiency after the optimization has increased by more than 100% over its baseline value. This drastic improvement in the wing performance is achieved by using the mathematically rigorous optimization methodology based on the adjoint formulation. Another important conclusion that can be drawn from this numerical experiment is that significant increase in the wing propulsive efficiency can be achieved without an appreciable change in the flapping frequency.

c. Combined shape-kinematics optimization

The last problem addresses a very important question on whether even higher performance gains are possible by including both shape and kinematic design variables into the optimization procedure, thus significantly expanding the design space that may contain extremum points with higher values of propulsive efficiency. For this optimization problem, the shape and kinematic design variables are identical to those used in the previous two cases. Thus, there are a total of 27 active variables including 19 shape and 8 kinematic parameters. The same upper and lower bounds on each design variable have been used to avoid nonphysical wing geometries and kinematics. Figure 6 shows the convergence history of the objective functional. Note that the convergence is slower and less monotonic as compared with the previous two cases. The optimizer performed 22 flow solutions

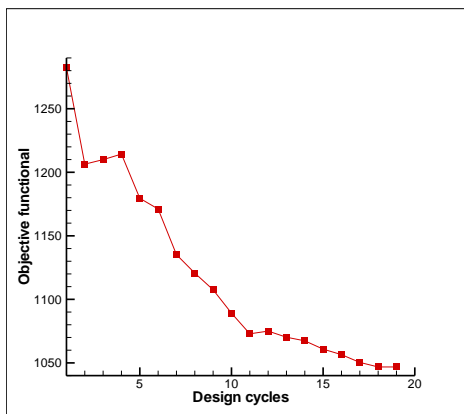


Figure 11: Convergence history of the objective functional.

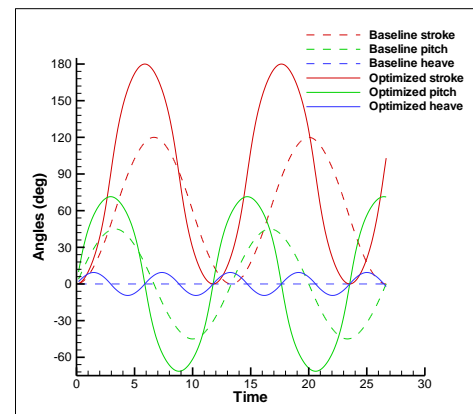


Figure 12: Baseline and optimal stroke, pitch and heave angle profiles.

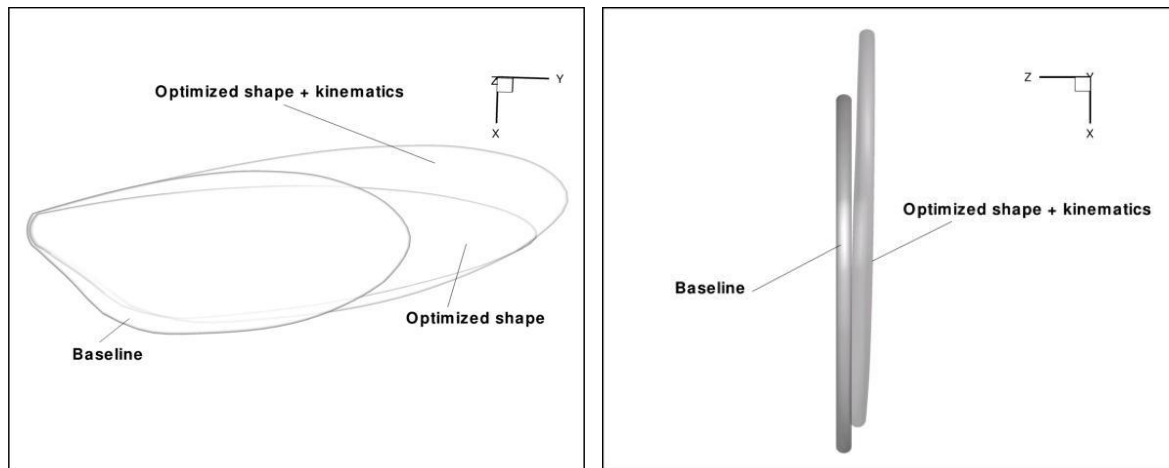


Figure 13: Planforms (left) and cross sections of the wing before and after combined optimization of shape and kinematics.

and 18 adjoint solutions for this test case. The final stroke, pitch, and heave angle profiles are depicted in Fig. 12. The optimization has not only increased the magnitude of the peaks of all three angles, but has also altered the frequency such that it has reached its upper bound. The stroke and pitch angle amplitudes have attained the values of 90° and 71° , which are practically identical to those obtained by optimizing the wing kinematics alone. Note, however, that the optimal stroke and pitch angle profiles significantly differ from those found in the previous case. The wing rotation for the current case occurs significantly faster at the end of upstroke and downstroke. Though the optimal solution of the combined shape-kinematics optimization problem also resembles a figure-eight stroke path, the heave angle amplitude is more than 50% less than its optimal value obtained in the previous optimization case. Note that the optimal wing kinematics found using the combined optimization strategy is similar to that observed in insects and hummingbirds, which is characterized by rapid wing rotation at the end of each stroke.

The baseline and optimized wing geometries are presented in Fig. 13. The span of the wing has increased by 41% after the combined optimization of wing shape and kinematics, which is even greater than that obtained by optimizing only the wing geometry. In contrast to the first test case, the mean chord length, wing tip profile, and twist have not been appreciably changed in the course of optimization. Another key distinction between the optimal geometries obtained in the first and current test cases is that the planform has been rotated such that the axis about which the wing pitches has been shifted towards the trailing edge and is located approximately at 50% of the chord. The simultaneous optimization of the wing shape and kinematics results in the optimal design that is considerably different from that found by optimizing the wing shape and kinematics independently, thus indicating that there is an essentially nonlinear relationship between these design variables.

Figure 14 presents snapshots of an iso-surface of q -criterion at four phase angles $\psi = 292.5^{\circ}, 315^{\circ}, 337.5^{\circ}, 360^{\circ}$ for the current problem. The combined optimization of the wing shape and kinematics significantly increases the size and strength of the leading- and trailing-edge vortices during the entire flapping motion including the rotation stage at the end of each stroke. The wing-wake interaction is also significantly stronger for the optimized configuration. The strengthening of the leading- and trailing-edge vortices drastically increases the thrust and propulsive efficiency generated by the optimized wing as one can see in Figs. 15 and 16. As follows from these figures, the combined optimization of the wing shape and its kinematics provides the largest increase in both the wing thrust and propulsive efficiency as compared with the previous two cases when the shape and kinematics have been optimized independently. The stroke-averaged thrust coefficient has been increased by about 70% and 380% over its value obtained by independently optimizing the wing kinematics and shape. The stroke-averaged propulsive efficiency demonstrates a similar behavior as evident in Fig. 16. All these results indicate that the optimization of wing kinematics and its shape should be performed in a coupled fashion to achieve the maximum improvement in flapping wing performance.

VII. Conclusions

The shape and kinematics of a hovering wing undergoing insect-based flapping motion have been optimized for maximum thrust and propulsive efficiency by using the time-dependent adjoint-based methodology developed in [13, 14]. In contrast to other optimization techniques, the adjoint formulation allows to compute the sensitivity derivatives with respect to all design variables at a cost comparable to that of a single flow solution, thus making the time-dependent optimization of 3-D turbulent flapping-wing flows feasible for practical applications. Three time-dependent optimization problems with the same objective functional have been

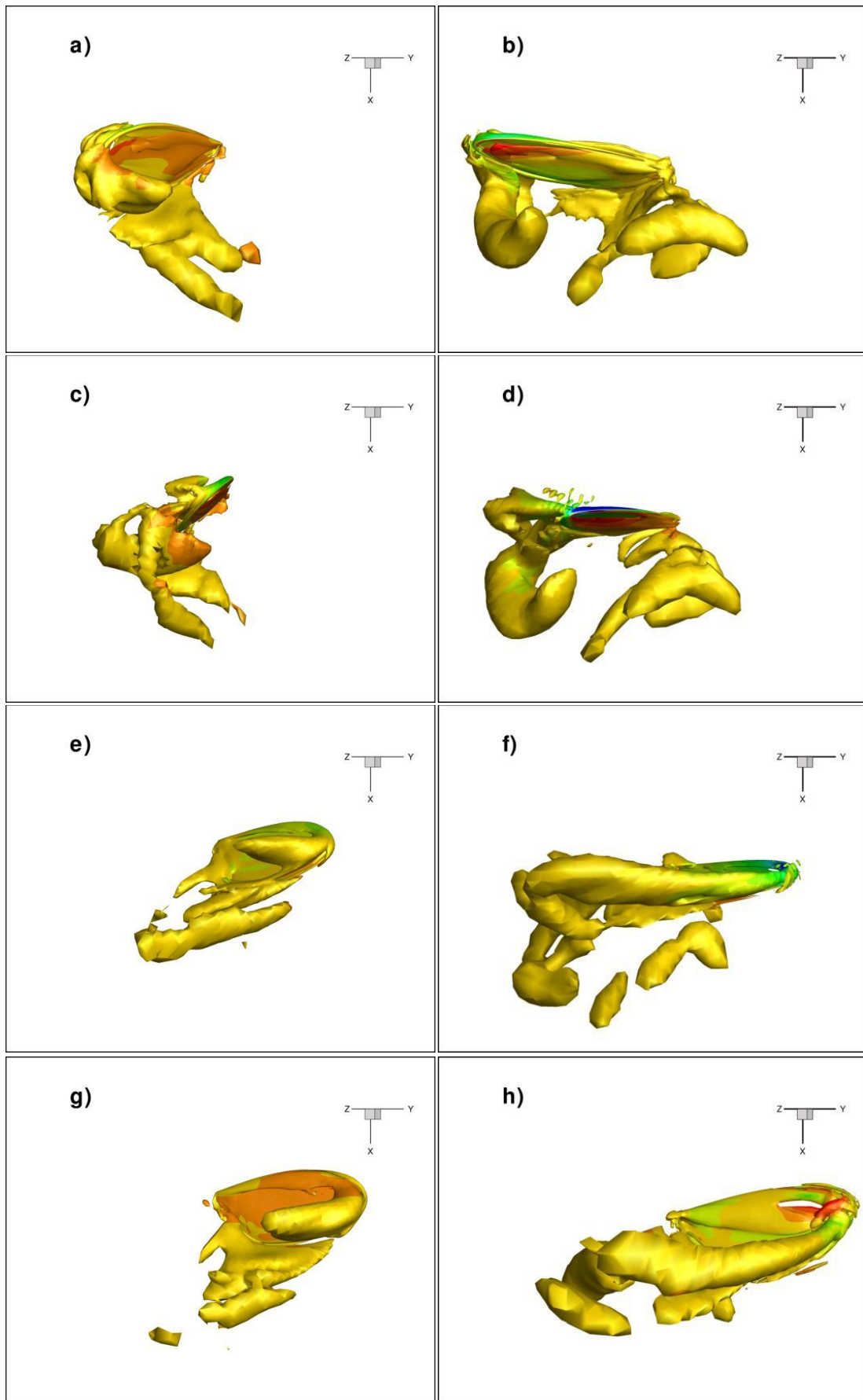


Figure 14: Iso-surface of the q -criterion at phase angles $\psi = 292.5^\circ, 315^\circ, 337.5^\circ, 360^\circ$ obtained for the baseline (left column) and optimized wing kinematics and geometry.

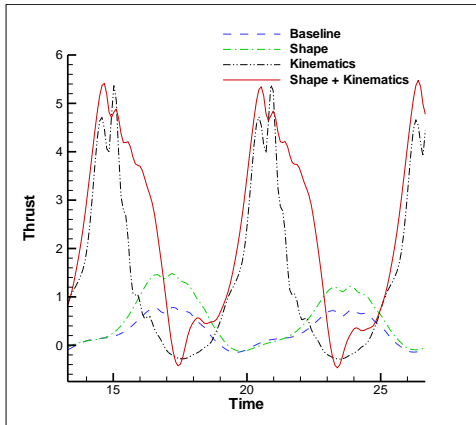


Figure 15: Baseline and optimal thrust profiles.

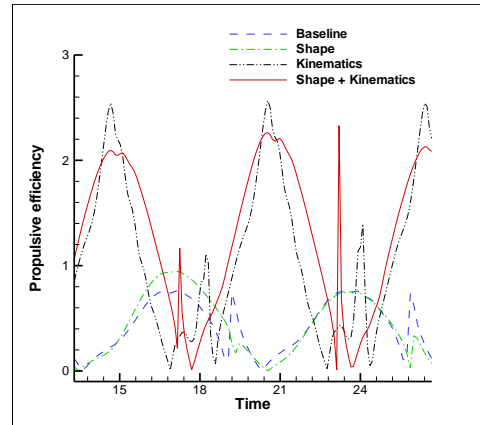


Figure 16: Propulsive efficiency before and after optimization of wing shape and kinematics.

considered. The first two cases optimize the wing shape and kinematics which are performed independently, while the third test case is based on the combined shape-kinematics optimization of the same baseline flapping wing. The objective functional has been defined such that it maximizes the wing thrust coefficient and minimizes the drag and consequently the power required for the wing operation. For the first optimization case, 19 variables including 12 planform and 7 twist parameters are used as design variables. The design variables for the second problem consists of 8 kinematic parameters including amplitude, frequency, shape, and symmetry of stoke, pitch and heave angle profiles. The design space of the third optimization problem consists of both shape and kinematic design variables defined in the first two cases. For each problem considered, the thrust coefficient has been significantly improved after the optimization as compared with its baseline value. Note, however, that the shape optimization alone is not as efficient as the other two optimization strategies. The mean values of the thrust coefficient obtained by independently optimizing the wing shape and its kinematics are about 90% and 500% higher than the baseline value, respectively. The simultaneous optimization of the wing shape and kinematics provides even further increase in the stroke-averaged thrust coefficient which is 70% greater than its maximum value obtained by the optimization of wing kinematics alone. Similar improvements in the stroke-averaged propulsive efficiency are observed for all three optimization problems considered. Our numerical results indicate that there are several factors that play the major role in improving the wing aerodynamic performance. First of all, the wing span and aspect ratio have been significantly increased by the shape and shape-kinematics optimization strategies. Note, however, that there have been no appreciable changes in the wing twist for all cases considered. The second common trend observed in our numerical experiments is that the stoke, pitch, and heave angle amplitudes and frequencies have been significantly increased during the optimization. Moreover, the stroke angle amplitude and all frequencies have reached their upper bound values. The third key distinction of the optimal solution from the baseline kinematics is that the optimized stroke path closely resembles a figure-eight shape observed in insects and hummingbirds. Another important conclusion that can be drawn from our results is that the optimized stroke and pitch angles are characterized by rapid changes during stroke reversals and significantly different from the corresponding baseline sinusoidal profiles. All these factors significantly increase the size and strength of the leading and trailing edge vortices both in the middle of each stroke and when the wing changes direction, thus increasing the pressure difference between windward and leeward sides of the wing. One of the main conclusions of this work is that the optimal solutions found by optimizing the wing shape and kinematics independently are quantitatively different from the optimal solution obtained by solving the optimization problem with the extended design space that includes both the shape and kinematic design variables. It gives us an indication that there is an essentially nonlinear relationship between the major kinematic parameters (amplitude, frequency, phase shift angle, etc.) and shape parameters (wing planform, twist thickness, etc.). These results show that the time-dependent adjoint-based methodology developed in [13, 14] is capable of significantly improving the flapping wing performance while satisfying the imposed constraints and can be used as a powerful tool for design and optimization of flapping-wing MAVs.

Acknowledgements

The authors would like to thank Eric Nielsen of NASA Langley Research Center for many helpful discussions pertaining to the current work and acknowledge the partial support from Army Research Laboratory through grant W911NF-06-R-006.

References

- [1] M. F. Platzer and K.D. Jones, "Flapping-wing Aerodynamics: Progress and Challenges," *AIAA Journal*, Vol. 46(9), pp. 2136-2149, 2008.
- [2] W. Shyy, H. Aono, K. Chimakurthi, P. Trizila, C K Kang, C E S Cesnik, H Liu, "Recent progress in flapping wing aerodynamics and aeroelasticity," *Progress in Aerospace Sciences*, Vol. 46(7), pp. 284-327, 2010.
- [3] P.-O. Persson, D. J. Willis and J. Peraire, *The Numerical Simulation of Flapping Wings at Low Reynolds Numbers*, AIAA Paper 2010-724, 2010.
- [4] R. Malhan, V.K. Lakshminarayan, J. Baeder, I. Chopra, "CFD investigation of aerodynamics of rigid flapping wings for MAV applications: Methodology validation ", *Pros. of the AHS Specialists Conference*, Jan 25-27, Tempe, 2011.
- [5] M. Jones and N. Yamaleev, "The effect of a gust on the flapping wing performance," *AIAA 2012-1080*, 2012.
- [6] Hamdaoui, J.-B. Mouret, S. Doncieux and P. Sagaut, *Optimization of Kinematics for Birds and UAVs using Evolutionary Algorithms*, *Proceedings of the World Academy of Science, Engineering and Technology*, Vol. 30, July 2008.
- [7] K. Ito, "Optimization of Flapping Wing Motion," *ICAS 2002 Congress*, 2002.
- [8] M. Milano, M. Gharib, "Uncovering the physics of flapping flat plates with artificial evolution," *J. Fluid Mech.*, Vol. 534, pp. 403-409, 2005.
- [9] M. Culbreth, Y. Allaneau, A. Jameson, "High-Fidelity Optimization of Flapping Airfoils and Wings," *AIAA P. 2011-3521*, 2011.
- [10] H. Tuncer and M. Kaya, *Optimization of Flapping Airfoils for Maximum Thrust and propulsive Efficiency*, *Acta Polytechnica*, Vol. 44, No. 1, 2004.
- [11] B. K. Stanford and P. S. Beran, "Cost reduction techniques for the design of non-linear flapping wing structures," *Int. J. Numer. Meth. Eng.* Vol. 88, pp. 533-555, 2011.
- [12] E. Nielsen, B. Diskin, "Discrete adjoint-based design for unsteady turbulent flows on dynamic overset unstructured grids," *AIAA P. 2012-0554*, 2012.
- [13] N. Yamaleev, B. Diskin, E. Nielsen, "Adjoint-based methodology for time-dependent optimization," *AIAA Paper 2008-5857*, 2008.
- [14] E. Nielsen, B. Diskin, N. Yamaleev, "Discrete adjoint-based design optimization of unsteady turbulent flows on dynamic unstructured grids," *AIAA J.*, Vol. 48, No.6, pp. 1195-1206, 2010.
- [15] R. T. Biedron and J. L. Thomas, "Recent Enhancements to the FUN3D Flow Solver for Moving Mesh Applications," *AIAA 2009-1360*, 2009.
- [16] Anderson, W. K., and Bonhaus, D. L., "Implicit/Multigrid Algorithms for Incompressible Turbulent Flows on Unstructured Grids," *J. Comput. Physics*, Vol. 128, No. 2, 1996, pp. 391-408.
- [17] Anderson, W. K., Rausch, R., and Bonhaus, D. L., "An Implicit Upwind Algorithm for Computing Turbulent Flows on Unstructured Grids," *Computers & Fluids*, Vol. 23, No. 1, 1994.
- [18] FUN3D official web site: <http://fun3d.larc.nasa.gov>
- [19] L. Kaufman and D. Gay, "PORT Library: Optimization and Mathematical Programming – User's Manual," Bell Laboratories, 1997.
- [20] Samareh, J. A., "A Novel Shape Parameterization Approach," *NASA TM-1999-209116*, May 1999.